Multibody System Dynamics (2006) 15: 351–372
DOI: 10.1007/s11044-005-9001-3

A Super-Element of Track-Wheel-Terrain Interaction for Dynamic Simulation of Tracked Vehicles

ZHENG-DONG MA and N. C. PERKINS
Department of Mechanical Engineering, The University of Michigan

(Received: 22 April 2004; accepted in revised form: 29 November 2004)

Abstract. A track-wheel-terrain interaction model is presented in this paper, which can be used as a "force" super-element in a multibody dynamics code for dynamic simulation of tracked vehicles. This model employs a nonlinear finite element representation for the track segment that is in contact with the terrain and roadwheels, which can be used to simulate two different track systems, namely a continuous rubber band track and a multi-pitched metallic track, provided the finite element mesh in the track model is properly defined. The new track model accounts for the tension variations along the track (due to the non-uniformly distributed normal pressure and traction), track extensibility, and geometrically large (nonlinear) track deflections. A new solution algorithm is then proposed that includes an adaptive meshing method for representing track movement during the simulation for the multi-pitch tracks. Doing so produces a track model that captures high-frequency content of the track-wheel-terrain interaction, and it can more accurately describe the mechanics of a multi-pitch track as the vehicle negotiates rough terrain. The resulting track-wheel-terrain model combines approximate and known constitutive laws for terrain response with the new track representation, which allows the computation of the normal and shear forces, as well as the passage frequency, at the track-terrain interface. The track model and solution algorithm are further illustrated in this paper using a simple two-wheel system model and a full vehicle model of an M1A1 tank.

Keywords: modeling and simulation, tracked vehicles, track-wheel-terrain interaction, dynamic systems, non-linear finite element, multibody systems

1. Introduction

A critical need in simulating the dynamic response of tracked vehicles is providing an effective model for representing track-wheel-terrain interactions. To capture the full coupling of the track-wheel-terrain interaction and the overall vehicle response, one can employ an iterative procedure at each integration time step as follows. First, approximate the positions and rotations of the roadwheels, and use these as the inputs to the track-wheel-terrain subsystem. Second, solve the track-wheel-terrain subsystem problem for the track contact forces resulting from the terrain and the roadwheels. Third, sum the reaction forces between the track and the roadwheels, and then apply these to the overall vehicle system to predict the dynamic response of the vehicle including the positions and rotations of the roadwheels. Next, the

predicted positions and rotations of the roadwheels are used as the corrected inputs for the track-wheel-terrain subsystem, and the subsystem problem is then solved again. Through iteration, this process converges to the dynamic response of the overall vehicle system for the given time step. Note that similar procedure is employed in the commercial multibody dynamics codes, such as ADAMS and DADS, to include the force elements (e.g., bushings, spring-damper-actuators, contact elements, and user-defined forces) in multibody dynamics simulation models. In this paper, we propose to develop a special force super-element for the track-wheel-terrain interface with a nonlinear finite element representation of the track. This force super-element can include the simplest unit of the track-wheel-terrain interface model or a more complete multi-wheel traction system model that can be solved independently. This force super-element can then be implemented in a general multibody dynamics code with various options as one (essential) component of a tracked vehicle model.

A literature review has been provided in [1] for the major efforts on modeling and simulation of tracked vehicles since nineteen fiftieth [see 2–18]. In [1], we have presented a track-wheel-terrain interaction model by introducing a continuous model for the track in contact with both the road wheels and the terrain. This model allows the track segment that is in contact with the terrain and roadwheels to deform into any physically feasible shapes, and it accommodates non-uniform track tension and the normal and shear stresses that develop at the track-terrain and track-wheel interfaces. Both contacts between the track and the roadwheels and the track and the terrain are treated in the same manner using a penalty method, which simplifies the solution procedure for the dynamic simulation. In this paper, we extend this track model with a non-linear finite element representation and a new strategy for adapting the finite element mesh during simulation. Doing so allows the track model to more accurately represent the response of a track with multiple pitches as the vehicle travels various terrains with varied speed. The continuous track model developed in [1] can be, therefore, reduced to a multi-finite-pitch track in this paper with improved accuracy. The comparisons between the results obtained with and without using the current track-wheel-terrain interaction model have shown the great effectiveness of using the current model. With the adaptive meshing, the new track-wheel-terrain interaction model can capture the pitch passage frequency and can be use to predict high-frequency content in the response of a track with multiple pitches. This enhanced track model has then been used to study the dynamics of a full vehicle model of an M1A1 tank and to demonstrate the generality of the track-wheel-terrain model developed in this paper, as well as to illustrate how the dynamics of this vehicle influence the response of the track in contact with the terrain.

2. Track-Wheel-Terrain Interaction Model

To capture the full coupling of the track-wheel-terrain interaction and the overall vehicle response, one can employ a force super-element in the multibody dynamic

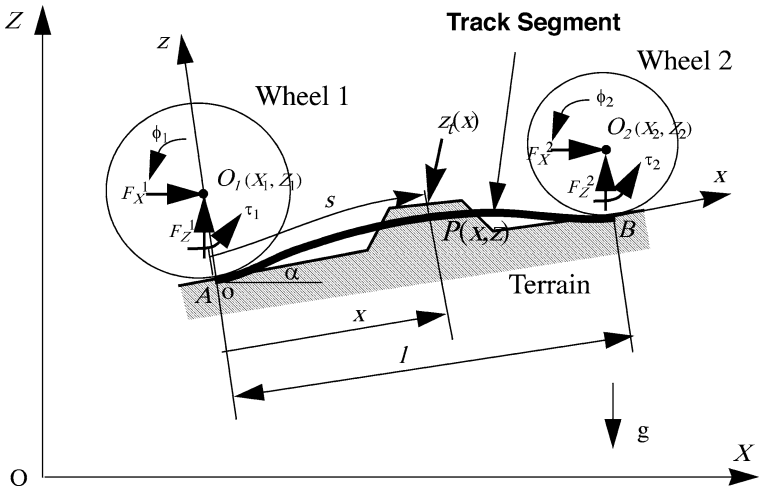

Figure 1. Force super-element for track-wheel-terrain interaction.

simulation. A schematic of an example force super-element is shown in Figure 1, and includes a track segment (which is considered as a rubber band track at this moment), two adjacent roadwheels, and the portion of the terrain between the roadwheels. (Note that this assumption can be extended to include several roadwheels as shown in the example provided in the last part of this paper.) In the current force super-element, the inputs to the force super-element are the locations (displacements) of the centers of the roadwheels O_1 and O_2 measured at the global coordinate system O-XYZ, i.e., (X_1, Z_1) and (X_2, Z_2), the angles ϕ_1 and ϕ_2 describing the orientations of any radial line in the plane of the roadwheels, and the profile of the terrain given by the function $z_t(x)$. The outputs of the force super-element are the forces and torques on the points O_1 and O_2 of the roadwheels, i.e., F_x^1, F_z^1, τ_1, F_x^2, F_z^2, τ_2. The domain of the track segment extends from point A to point B which lies along the common tangent to the roadwheels. It is assumed that the track does not slip at A or B relative to the roadwheels. As a result, the domain of the undeformed track segment not in contact with the roadwheels is $L = l + r_1\phi_1 - r_2\phi_2$, where l denotes the distance between points A and B, and r_1 and r_2 are the radii of the roadwheels 1 and 2, respectively. Note that the no-slip condition could be relaxed by considering frictional contact between the track and the roadwheels. The force super-element formulated herein permits one to compute the deflection of a continuous track segment, treating both the terrain and roadwheels as deformable contacting media.

Figure 2 shows the equilibrium of an infinitesimal track element in the local coordinate system o-xyz which is also shown in Figure 1. Assume that track inertia effects are sufficiently damped by the (tremendous) dissipation at the track/terrain interface that they can now be ignored in this region. Assume also that the track can be modeled as a one-dimensional flexible continuum obeying a linearly elastic constitutive law for extension. The resulting track equilibrium equation is then

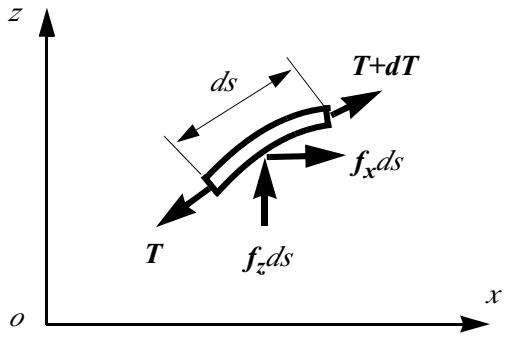

Figure 2. Equilibrium of an infinitesimal track element.

obtained as (refer to [1])

$$-\frac{\partial}{\partial s}\left(\hat{T}\frac{\partial \mathbf{y}}{\partial s}\right) = \mathbf{f} \tag{1}$$

where, $\mathbf{y} = \{x, z\}^T$ denotes the position vector of the track at point P in o-xyz, s denotes the curvilinear coordinate of P along the track as shown in Figure 1, $\mathbf{f} = \{f_x, f_z\}^T$ denotes the force/length distributed along the track, where f_x and f_z are the components applied along the x and z directions, respectively, and $\hat{T}$ is a tension measure given by

$$\hat{T} = \frac{EA \cdot T}{EA + T} \tag{2}$$

Here, EA denotes the stiffness of a unit length of track and T is the (non-uniform) track tension. Note that Equation (1) can be extended to include the track inertia effects by adding a dynamic term, $-m\frac{\partial^2 \mathbf{y}}{\partial t^2}$, in the right side of the equation.

Equation (1) results in a two-point nonlinear boundary value problem. To solve it, an incremental form of the track model is obtained by assuming $\mathbf{y} = \mathbf{y}_0 + \Delta\mathbf{y}$, $\hat{T} = \hat{T}_0 + \Delta\hat{T}$, and $\mathbf{f} = \mathbf{f}_0 + \Delta\mathbf{f}$, where $\mathbf{y}_0$ is an approximate solution of Equation (1) obtained from a prior iteration with associated tension measure $\hat{T}_0$ and loading $\mathbf{f}_0$. Updated solutions are then sought in the forms

$$-\frac{d}{ds}\left(\mathbf{B}\frac{d}{ds}\Delta\mathbf{y}\right) - \mathbf{G}\Delta\mathbf{y} = \mathbf{r} \tag{3}$$

where

$$\mathbf{B} = \hat{T}_0\left(\mathbf{I} + \frac{EA}{T_0^3}\mathbf{T}_0\mathbf{T}_0^T\right) \tag{4}$$

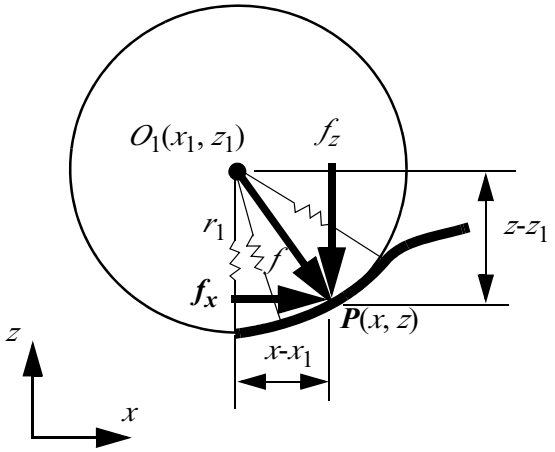

Figure 3. Track-wheel contact.

$$\mathbf{G} = \left.\frac{\partial \mathbf{f}}{\partial \mathbf{y}}\right|_{\mathbf{y}=\mathbf{y}_0} \tag{5}$$

and

$$\mathbf{r} = \mathbf{f}_0 + \frac{d}{ds}\left(\hat{T}_0 \frac{d\mathbf{y}_0}{ds}\right) \tag{6}$$

is the residual obtained at the last iteration step. In Equation (4), $\mathbf{T}_0 = \{H_0, V_0\}^T$ denotes the tension vector, where H_0 and V_0 are the components of the tension vector along x and z directions, respectively. The magnitude of the tension is $T_0 = \sqrt{H_0^2 + V_0^2}$.

Note that f_x and f_z include the self weight of the track and the normal and shear stresses from the terrain and/or roadwheels. The normal and shear stresses are functions of the relative deformation of the track and the terrain, and the track and the roadwheels, as described next.

As depicted in Figure 3, each roadwheel is modeled as a stiff elastic element with compliance in the radial direction. Here, (x_1, z_1) are the local coordinates of the point O_1 in o-xyz, r_1 is the radius of the roadwheel, and f is the normal force/length acting radially outwards at the arbitrary point P of the track.

$$f = \begin{cases} -k_w(r - r_1) \text{ for } r < r_1 \\ 0 \qquad\quad \text{for } r \geq r_1 \end{cases} \tag{7}$$

The quantity k_w represents the roadwheel/track contact stiffness, and $r = \sqrt{(x - x_1)^2 + (z - z_1)^2}$. Note that $f_x = \frac{1}{r}(x - x_1) f$ and $f_z = \frac{1}{r}(z - z_1) f$.

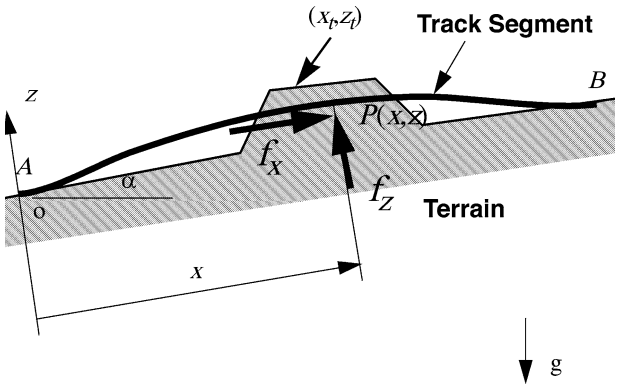

Figure 4. Track-terrain contact.

As depicted in Figure 4, the track also contacts the terrain beneath each road-wheel and may also contact the terrain along portions in between. The normal force/length acting along the z axis of the local o-xyz frame, and the traction force/length along the x axis produced by terrain contact and weight are

$$f_x = \tau_1 W - mg \sin\alpha \quad \text{and} \quad f_z = P_1 W - mg \cos\alpha \tag{8}$$

where W denotes the track width, mg denotes the track weight/length, α is the angle between axes o-x and O-X as shown in Figure 1, and

$$\tau_1 = \begin{cases} \tau(x, z) & \text{if } z < z_t \\ 0 & \text{if } z \geq z_t \end{cases} \tag{9}$$

$$p_1 = \begin{cases} p(z) & \text{if } z < z_t \\ 0 & \text{if } z \geq z_t \end{cases} \tag{10}$$

Here (x_t, z_t) is the terrain profile in the local coordinate system. Here, $\tau = \tau(x, z)$ and $p = p(z)$ are determined by the particular shear stress-shear displacement relationship and pressure-sinkage relationship adopted for the terramechanics model. For example, if we employ the Janosi-Hanamoto equation [19] for the shear stress-shear displacement relationship, then

$$\tau(x, z) = -\text{sgn}(\Delta)\tau_m \left[1 - \exp\left(-\frac{|\Delta|}{K}\right)\right] \tag{11}$$

where Δ is the shear displacement, K is the shear modulus, and τ_m is the maximal shear stress given by

$$\tau_m = C + \sigma \tan\phi \tag{12}$$

Here, C denotes the cohesive strength of the soil, $\sigma = p_1$ is the normal stress, ϕ is the angle of internal friction.

Similarly, if we employ Bekker's equation [3] for the pressure-sinkage relationship, then

$$p(z) = \left(\frac{k_c}{W} + k_\phi\right)(z_t - z)^n \quad \text{for } z \le z_t \tag{13}$$

where k_c denotes the soil cohesiveness coefficient, k_ϕ denotes the soil internal friction coefficient, and n is the pressure-sinkage exponent.

Note that other terramechanics laws can readily be substituted for the example laws given above. For example, the pressure-sinkage relationship might also consider repeated loading [12, 13].

3. Finite Element Discretization and Adaptive Mesh

The weak form of Equation (3) is

$$\int_0^1 \delta \mathbf{w}'^T \mathbf{B} \Delta \mathbf{y}' ds - \int_0^1 \delta \mathbf{w}^T \mathbf{G} \Delta \mathbf{y} ds = \int_0^1 \delta \mathbf{w}^T \mathbf{f}_0 ds - \int_0^1 \hat{T}_0 \, \delta \mathbf{w}'^T \mathbf{y}_0' ds \tag{14}$$

where $\delta \mathbf{w}$ denotes a virtual displacement, and a prime denotes differentiation with respect to s.

A finite element method is then employed to discretize Equation (14) using linear interpolation functions. This choice not only simplifies the formulation, it also has the added advantage of immediately modeling a multi-rigid-link track (as opposed to a rubber band track). We will return to this point later as we review results.

As depicted in Figure 5, the track segment is divided into n_{el} finite elements, where n_{el} may be sufficiently large to model the track as a continuous belt, or restricted to a number equal to the number of the pitches in the track segment. In the latter case, each finite element corresponds to a single track pitch. Element i has two nodes with the coordinates $\{x_i, z_i\}$ for the left node and $\{x_{i+1}, z_{i+1}\}$ for the right node, where $i = 1, 2, \wedge, n_{el}$. The interpolation function

$$\Phi = \begin{bmatrix} \phi_1 & 0 & \phi_2 & 0 \\ 0 & \phi_1 & 0 & \phi_2 \end{bmatrix} \tag{15}$$

is composed of the linear functions

$$\phi_1 = \frac{1}{d_i}(s_{i+1} - s), \; \phi_2 = \frac{1}{d_i}(s - s_i), \; d_i = s_{i+1} - s_i \tag{16}$$

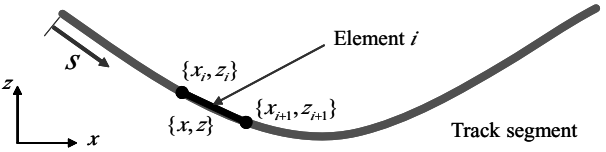

Figure 5. Finite element model.

where $s_i (i = 1, 2, \ldots, n_{el} + 1)$are coordinates of the nodes in the track curvilinear coordinate system. Thus, we form

$$\Delta \mathbf{y} = \Phi \mathbf{u}^{\mathrm{i}} \tag{17}$$

for $s \in [s_{\mathrm{i}}, s_{i+1}]$ where, $\mathbf{u}^i = \{\Delta x_i, \Delta z_i, \Delta x_{i+1}, \Delta z_{i+1}\}^{\mathrm{T}}$ is the vector of nodal variable perturbations for the i-th element. Then the i-th elementary stiffness matrix becomes

$$\mathbf{k}^e = \frac{1}{d}\begin{bmatrix} b_{xx} & b_{xz} & -b_{xx} & -b_{xz} \\ b_{xz} & b_{zz} & -b_{xz} & -b_{zz} \\ -b_{xx} & -b_{xz} & b_{xx} & b_{xz} \\ -b_{xz} & -b_{zz} & b_{xz} & b_{zz} \end{bmatrix} - \begin{bmatrix} c_{11} & c_{12} & c_{13} & c_{14} \\ c_{12} & c_{22} & c_{14} & c_{24} \\ c_{13} & c_{14} & c_{33} & c_{34} \\ c_{14} & c_{24} & c_{34} & c_{44} \end{bmatrix} \tag{18}$$

where

$$b_{xx} = \hat{T}_0 \left(1 + EAH_0^2/T_0^3\right),$$

$$b_{xz} = \hat{T}_0 \left(EAH_0V_0/T_0^3\right),$$

$$b_{zz} = \hat{T}_0 \left(1 + EAV_0^2/T_0^3\right),$$

$$c_{11} = \int_{S_i}^{S_{i+1}} g_{xx}\phi_1^2 ds, \quad c_{12} = \int_{S_i}^{S_{i+1}} g_{xz}\phi_1^2 ds, \quad c_{22} = \int_{S_i}^{S_{i+1}} g_{zz}\phi_1^2 ds,$$

$$c_{13} = \int_{S_i}^{S_{i+1}} g_{xx}\phi_1\phi_2 ds, \quad c_{14} = \int_{S_i}^{S_{i+1}} g_{xz}\phi_1\phi_2 ds, \quad c_{24} = \int_{S_i}^{S_{i+1}} g_{zz}\phi_1\phi_2 ds,$$

$$c_{33} = \int_{S_i}^{S_{i+1}} g_{xx}\phi_2^2 ds, \quad c_{34} = \int_{S_i}^{S_{i+1}} g_{xz}\phi_2^2 ds, \quad c_{44} = \int_{S_i}^{S_{i+1}} g_{zz}\phi_2^2 ds,$$

and g_{xx}, g_{zz}, and g_{xz} are components of the matrix $\mathbf{G}$ (defined in Equation (5)), i.e., $\mathbf{G} = \begin{bmatrix} g_{xx} & g_{xz} \\ g_{xz} & g_{zz} \end{bmatrix}$. The elementary residual vector is obtained as

$$\mathbf{r}^e = \begin{Bmatrix} f_x^i \\ f_z^i \\ f_x^{i+1} \\ f_z^{i+1} \end{Bmatrix} - \frac{\hat{T}}{d} \begin{Bmatrix} x_{i+1} - x_i \\ z_{i+1} - z_i \\ x_i - x_{i+1} \\ z_i - z_{i+1} \end{Bmatrix} \tag{19}$$

where

$$f_x^i = \int_{S_i}^{S_{i+1}} \phi_1 f_x ds,$$
$$f_z^i = \int_{S_i}^{S_{i+1}} \phi_1 f_z ds,$$
$$f_x^{i+1} = \int_{S_i}^{S_{i+1}} \phi_2 f_x ds,$$
$$f_z^{i+1} = \int_{S_i}^{S_{i+1}} \phi_2 f_z ds,$$

and $\{x_i, z_i, x_{i+1}, z_{i+1}\}^T$ is the elementary nodal displacements obtained at the last iteration step. Upon assemble, the incremental equation for the residual becomes

$$\mathbf{KU} = \mathbf{R} \tag{20}$$

where $\mathbf{K}$ is the global stiffness matrix, $\mathbf{U}$ is the global perturbation vector for the nodal variables, and $\mathbf{R}$ is the global residual vector.

Note that since linear interpolation functions, ϕ_1 and ϕ_2, are used for the finite element discretization, the track model (developed for a continuous element) can also describe a multi-pitch model of the track by matching the length of each finite element to the size of the track pitch. In this case, each pitch is also extensible and this captures the compliance introduced by the rubber bushings commonly used in connecting adjacent pitches. The track pitch is otherwise rigid and it is permitted to rotate about the pin connections (i.e., the descretization does not impose derivative continuity for the track deflection shape). Moreover, the pitch length determines the locations of the nodes (which represent the pin joints) these influence the pressure distribution. These joints also move relative to the local coordinate system *o-xyz* and their movement is captured herein using an adaptive finite element mesh at each time step during integration. For the rubber band track applications, if a fine mesh is used with an enough number of elements (about 20 in this case), an accurate representation can also be obtained. In Section 4.1, we will provide an example to show how easy to convert a multi-pitch track to a band track and the effect of this conversion.

To illustrate the adaptive meshing scheme, let θ_1 be the rotation angle of the first roadwheel as depicted in Figure 6, r_1 be the radius of the first roadwheel, d be the pitch length, and d_1 be the length of the first finite element of the track. Then d_1 is computed by

$$d_1 = \text{mod}\,(r_1\theta_1, d) \tag{21}$$

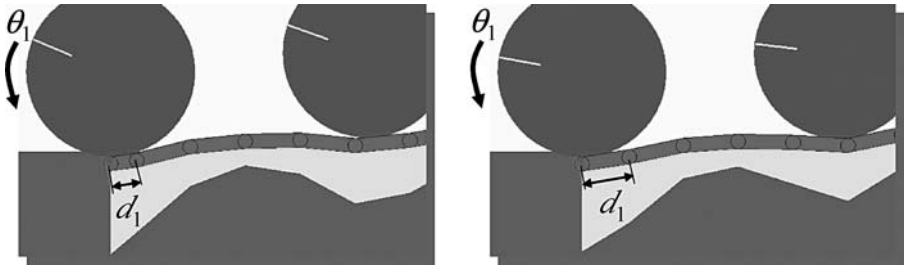

Figure 6. Adaptive meshing.

where mod is an operation that calculates the remainder of the arguments. Note that the length of the other finite elements in the track model will be d, except the length of the last finite element which is

$$d_{n_{el}} = \text{mod}\,(L - d_1, d) \tag{22}$$

where L is the total (undeformed) length of the track segment. Also, note that the system equation will become singular if d_1 approaches to zero. Therefore, a small threshold (e.g., $d_0 = 0.1d$) needs to be set, and to use $d_1 = d_0$ when $d_1 < d_0$. In the following section, we will illustrate the feasibility and applicability of the formulations developed in above through two examples: one is a simple two-wheel system; the other is a full vehicle system.

4. Examples

4.1. TWO-WHEEL EXAMPLE

Figure 7 illustrates a two-wheel track-wheel-terrain interaction model contacting a LETE sand terrain with a trapezoid bump on the top. This example is used to demonstrate the generality of the proposed approach to cover both rubber band and multi-pitch tracks and to demonstrate the difference of the predicted responses when a different number of track elements are used in the finite element discretization. The model in the left side of Figure 7 represents a system with a band track (continuous track), while the model in the right side represents that with a multi-pitch track, which has 6 individual links. Figure 7-a shows the two systems before the contact with the predicted sag under its own weight, while Figure 7-b shows the two systems in contact with the terrain, which also shows the predicted ground pressure beneath the track (in yellow color). For the purpose of comparison, it is assumed that the both tracks (continuous and multi-pitch tracks) have the same mechanical properties and the same length at the initial stage. Also, for the two models in Figure 7-b, the roadwheels experience the same sinkage for both cases. It is seen in Figure 7-b that

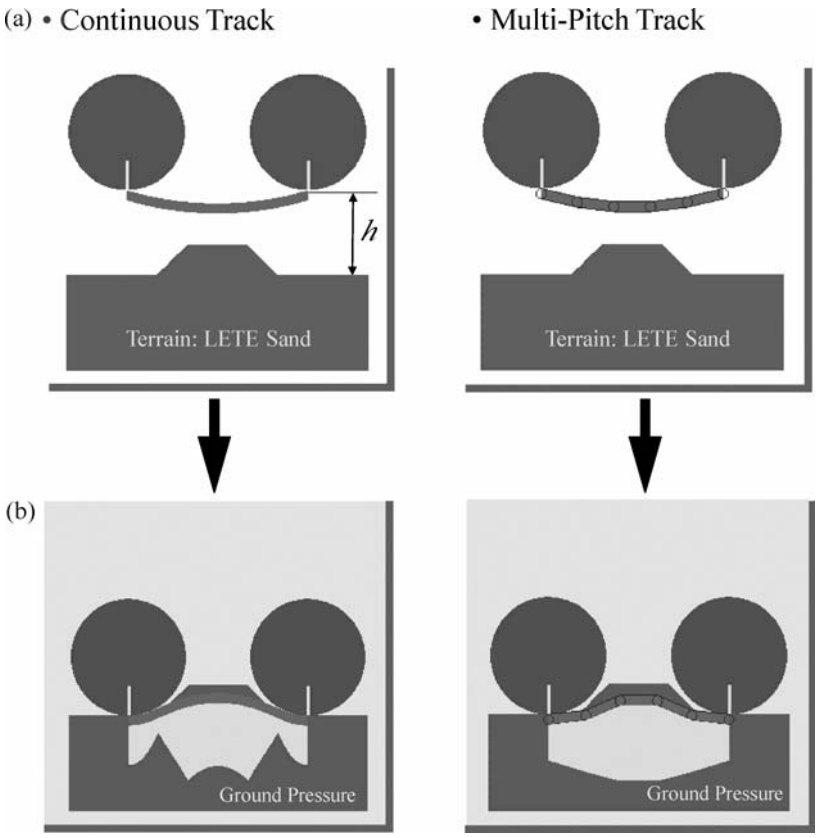

Figure 7. Comparison of two-wheel track-wheel—terrain interaction models.

Table I. Effect of the track type on the predicted forces.

Type of track	Tension (lbs)	F_x (lbs)	F_z (lbs)
Band	0.188e6	0.153e6	0.110e6
Multi-pitch	0.208e6	0.138e6	0.442e6

the track model developed can be used to simulate both the band track (using 6 finite elements) and the multi-pitch track (using 100 finite elements), and significantly different ground pressure distributions can be obtained when different track models are employed. Note that a 20 element model can also provide converged result with ignorable difference (compare to the 100 element model) for the continuous track. Table 1 further compares the net forces predicted using the two different track models. It is seen that while the predicted tensions and longitudinal forces are relatively close for the two models, the vertical forces are quite different. This difference is almost as large as 4 times. This indicates the importance to have a general model that can simulate both the different track systems.

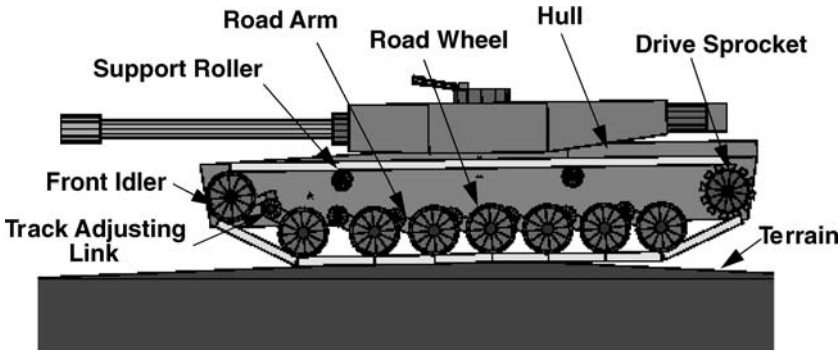

Figure 8. A two-dimensional full vehicle model of M1A1 tank.

4.2. A FULL VEHICLE EXAMPLE

A two-dimensional full vehicle model of M1A1 tank was developed in [17, 18] with the use of a simplified track-wheel-terrain interaction model. Figure 8 shows a schematic of the vehicle model developed. The major components of the vehicle system included the hull, a track, a front idler, a track adjusting mechanism, a drive sprocket, two support rollers, and seven pairs of road arms and roadwheels.

In references to [16–18], a modal representation of the track dynamics was employed. To this end, each track span was represented by four types of component modes: (1) a rigid body mode, (2) a constraint mode, (3) longitudinal vibration modes, and (4) transverse vibration modes. The rigid body mode describes the superimposed translation speed, and the constraint mode describes the static track elongation. The longitudinal and transverse vibration modes describe dynamic deformation about the sagged and translating equilibrium state. The resulting track equations were integrated with the other components in the vehicle system by developing a new general-purpose "force element" of track vibration for the commercial code DADS.

The full vehicle model was then simulated (within DADS) to study the response of the vehicle on rough terrain. Figure 9 shows a specific terrain profile used for this purpose (commonly referred to as "Profile 4"). Figure 10 shows the computed vehicle speed that results under a prescribe torque to the drive sprocket while traversing this terrain profile. As shown in Figure 10, the vehicle starts from rest and accelerates to a speed of approximately 25 mph near the end of this run. As an example output, Figure 11 illustrates the computed vertical displacements of the central (4-th) roadwheel at the roadwheel axis and the vehicle center of mass. In this paper we shall now use these computed response of the roadwheels to estimate the traction and pressure exerted by the terrain in the track using the track-wheel-terrain interaction model describing in following.

Figure 12 illustrates a seven-wheel track-wheel-terrain interaction model developed in this paper for estimating the traction and pressure exerted on the track. The

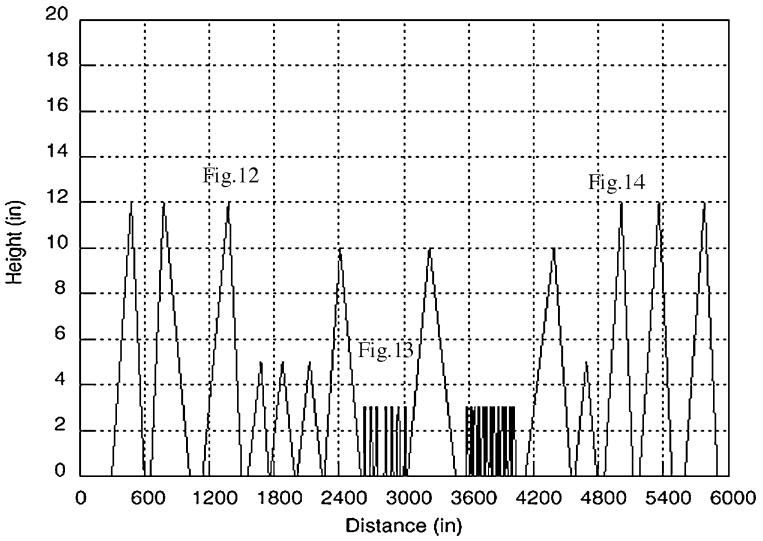

Figure 9. Example terrain profile (Profile 4). Figure numbers cross reference Figures in Results section.

parameters for the M1A1 tank are used to describe the track and roadwheel geometry. An example terrain is selected, namely LETE sand [1] with the terramechanics model of Equations (11) and (13). The track segment considered herein extends from the first roadwheel to the last roadwheel and it is assumed that there is no slip between the track and the first and last roadwheels. Thus, the total (stretched) length of the track segment is determined by the initial length of the segment and the relative rotation between the first and last roadwheels.

This track segment is decomposed into a total 24 finite elements. Each finite element represents one track pitch. The results reported next were computed using two meshes, a constant mesh and the adaptive mesh describe above.

Figures 13–16 illustrate snapshots from an animation of the track segment as the vehicle traverses the bump course. The normal pressure distribution (in yellow color) on the ground due to the passing track segment is illustrated together with the position and orientation of each road wheel and track pitch. Figure 13 illustrates the track segment as the vehicle traverses the second bump in the course and at low speed; refer to Figure 9 where a cross reference is made to Figure 13. This second bump is broad in that its base is comparable to the length of the track segment. Figure 13a–c illustrate the segment and resulting ground pressure as the vehicle ascends, summits and descends the bump, respectively. Figure 14 illustrates the segment as it traverses a sequence of small bumps and at moderate speed; refers again to Figure 9 and the cross reference to Figure 14. These small bumps lead to track bridging whereby portions of the track no longer contact the terrain. Figure 15 illustrates the track segment and ground pressure as the vehicle traverses the last bump in the

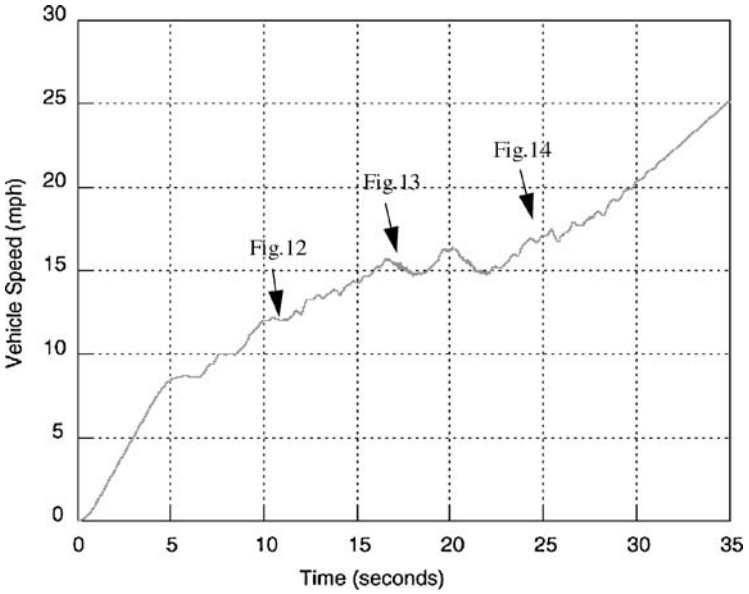

Figure 10. Vehicle speed predicted while traversing Profile 4 under constant (prescribed) drive torque.

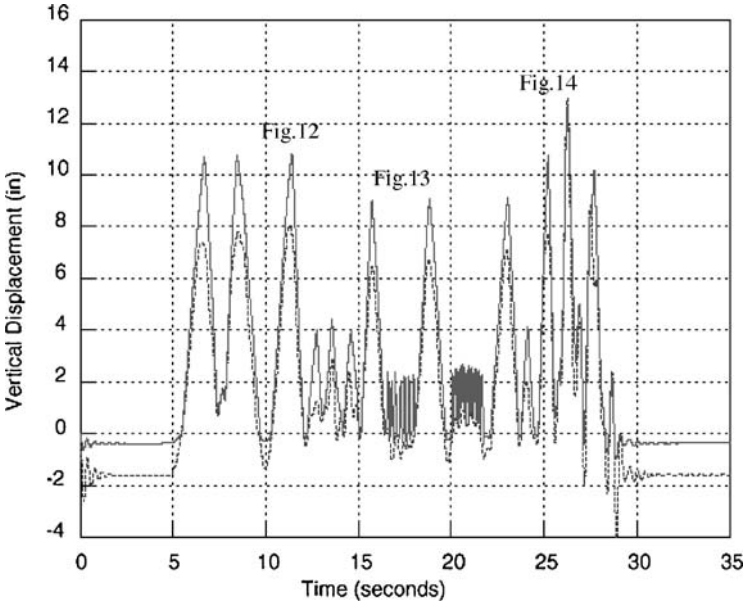

Figure 11. Vertical displacements of the 4-th roadwheel and the vehicle center of mass. Solid line represents 4-th roadwheel; dashed line represents vehicle center of mass.

Figure 12. Track-wheel-terrain interaction model with seven roadwheels for an M1A1 tank.

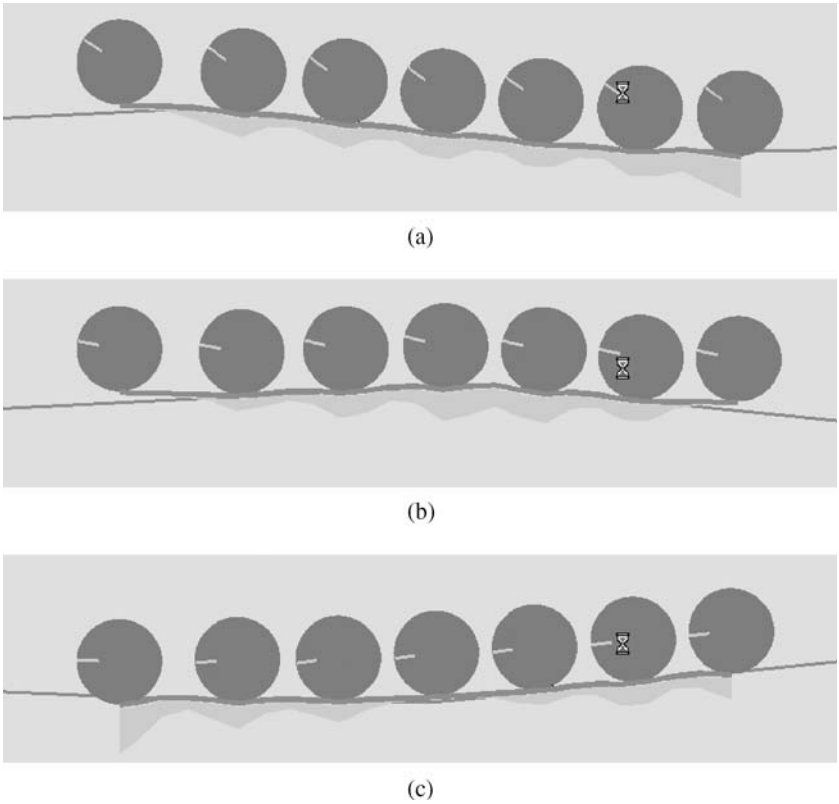

Figure 13. Normal pressure distribution on the terrain for an M1A1 traversing a broad bump at low speed, approximately 10 mph: (a) ascending, (b) summiting, (c) descending.

course. Like the second bump, the last bump is broad but here the vehicle speed is appreciable (approximately 20 mph). As shown in Figure 15-a, the ground pressure nearly vanishes as the vehicle is loosing contact with the terrain while ascending this bump. This is also accompanied by a large counterclockwise pitching of the vehicle that abruptly ends as it impacts the terrain while summiting and then descending the bump. This impact leads to the large ground pressures observable in Figures 15-b and 15-c. Figure 16 further illustrates a zoomed-in result for the track under the first two roadwheels.

Figure 17 provides a time history of the vertical reaction on the central (4th) roadwheel as the vehicle traverses the bump course. The largest reactions exist

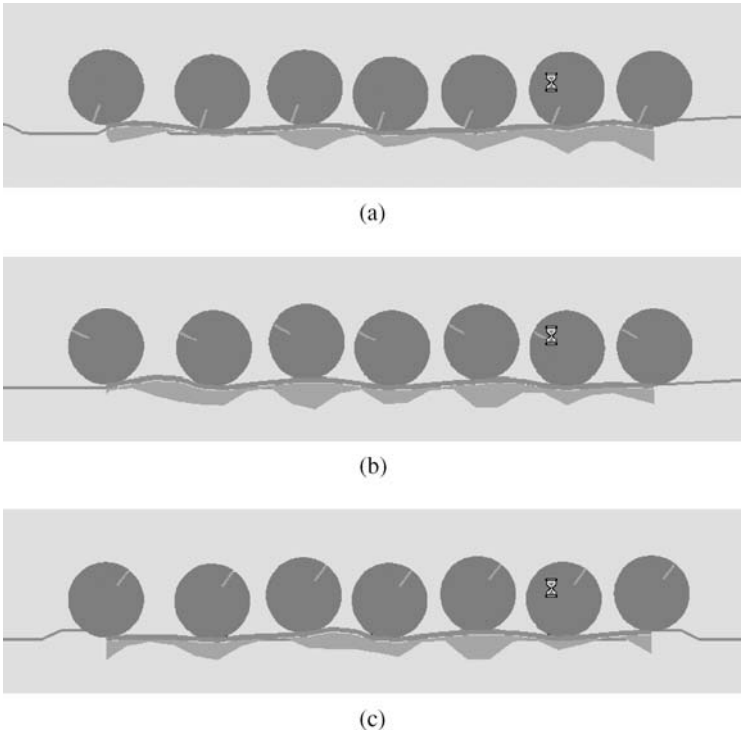

Figure 14. Normal pressure distribution on the ground: M1A1 tank traversing small obstacles at moderate speed, approximately 15 mph.

between 25–30 seconds as the vehicle encounters the final bump and at appreciable speed; refer to Figure 15. The next largest reactions occur between 15–20 seconds as the vehicle negotiates the small and closely spaced bumps apparent in Figure 14. These bumps induce high frequency reactions of the roadwheel and include frequencies that correspond to the track pitch passage frequency. Figure 18 further illustrates the frequency contents of the time history shown in Figure 17. It is seen that rich information is contained in the simulation result, which can be used to, for example, predict seismic signatures of the vehicle.

Attention will now focus on comparing the results above with results obtained using three qualitatively different models for track-terrain interaction. The other models include (1) one that models a continuous track (or band track) using a mesh of 150 elements (in contrast to 24 elements for discrete pitches), (2) a multi-body track (or multi-pitch track) using a mesh of 24 elements but without adaptive meshing, and 3) with a very stiff track (10 times stiffer than nominal) that approximates the inextensible track models used in prior studies [e.g., Reference 15]. For the sake of comparison, we will focus on the response of the track on the small obstacles at moderate speed considered above. In addition, we will report here the vertical

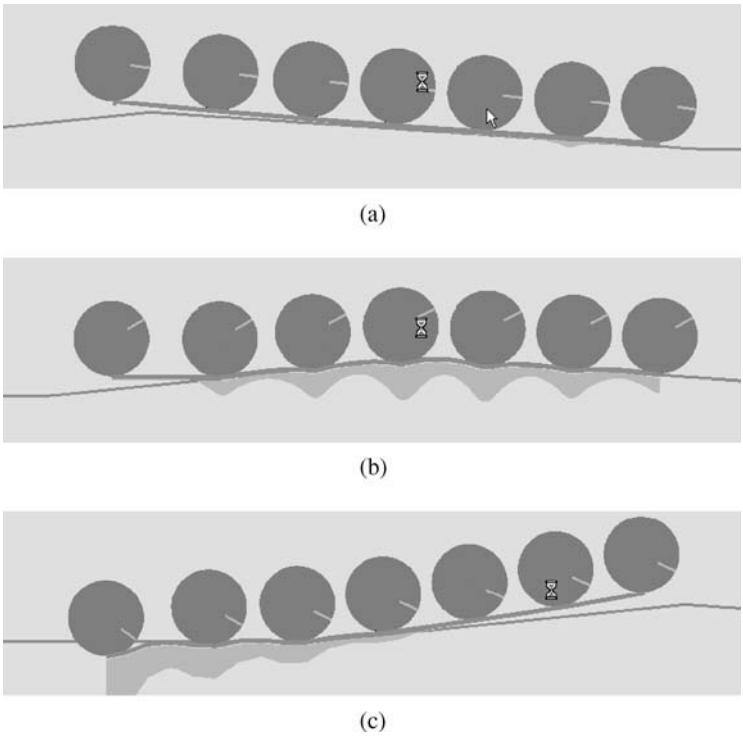

Figure 15. Normal pressure distribution on the ground: M1A1 tank traversing a broad bump at higher speed, approximately 20 mph. (a) ascending, (b) summiting, (c) descending.

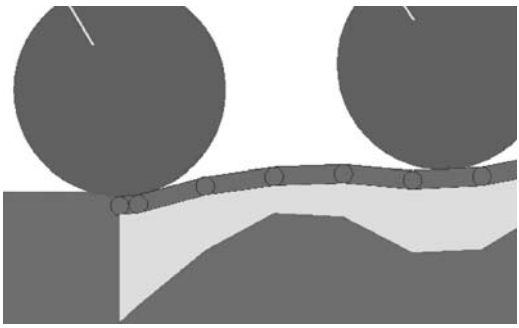

Figure 16. Zoomed-in result for the track under the first two roadwheels.

force generated at the central roadwheel as shown in Figure 17. The small obstacles considered correspond to that portion of Figure 17 from 15 seconds to 20 seconds.

Figure 19 shows the comparison with the continuous track (150 finite elements). As expected, the (structurally softer) continuous track model under-predicts the roadwheel reaction force and it also fails to capture the high frequency components

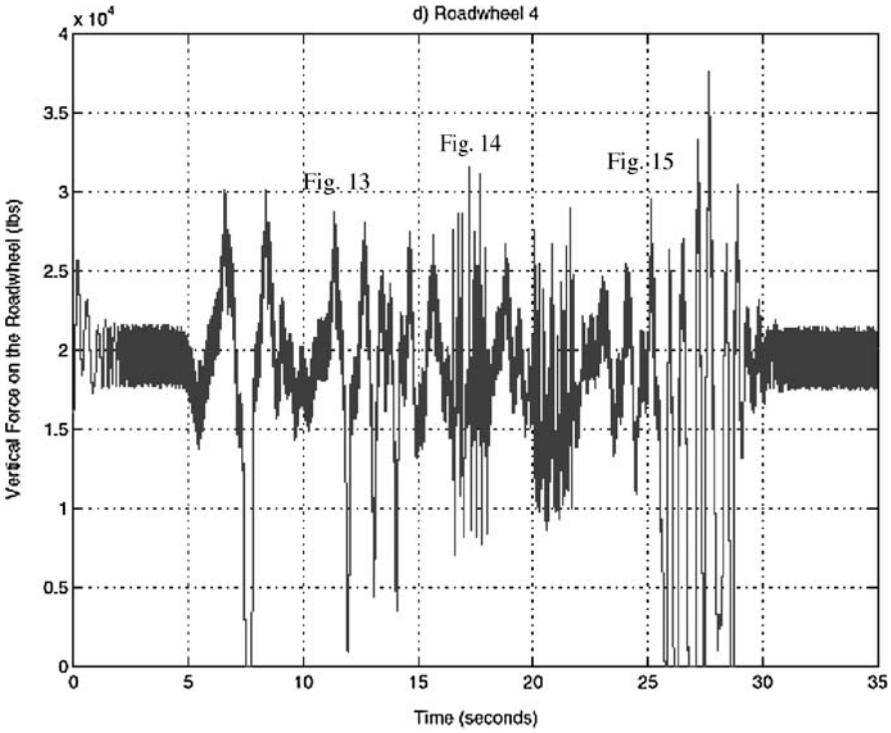

Figure 17. History of vertical force on the central (4-th) roadwheel for M1A1 traversing profile 4. Figure numbers refer to portions of bump course detailed Figures 13–15.

that result from the pitch passage frequency. Figure 20 shows the comparison with the results obtained with and without adaptive meshing. Without adaptive meshing, the model over-predicts the roadwheel reaction and again misses the high frequency components produced by the pitch passage frequency. Figure 21 shows the comparison with a very stiff track that approximates an inextensible track. The inextensible track model leads to significant over estimates of the roadwheel reaction as expected. This reinforces the conclusion that track extensibility must be accounted for in dynamic track models.

5. Conclusions

A track-wheel-terrain super-element is presented in this paper using a nonlinear finite element representation of the track segment and an adaptive meshing scheme. The super-element can be used in a multibody dynamic code for dynamic simulation of tracked vehicles, which covers from a rubber band track to a multi-pitched metallic track with rubber bushings. The track model accounts for the tension variations along the track, track extensibility, and geometrically large nonlinear

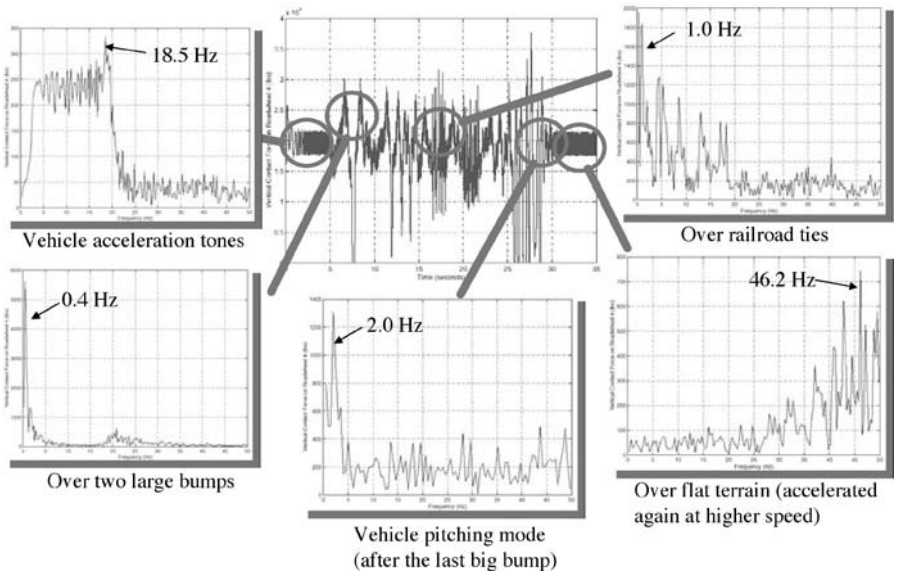

Figure 18. Frequency contents of the time history shown in Figure 17.

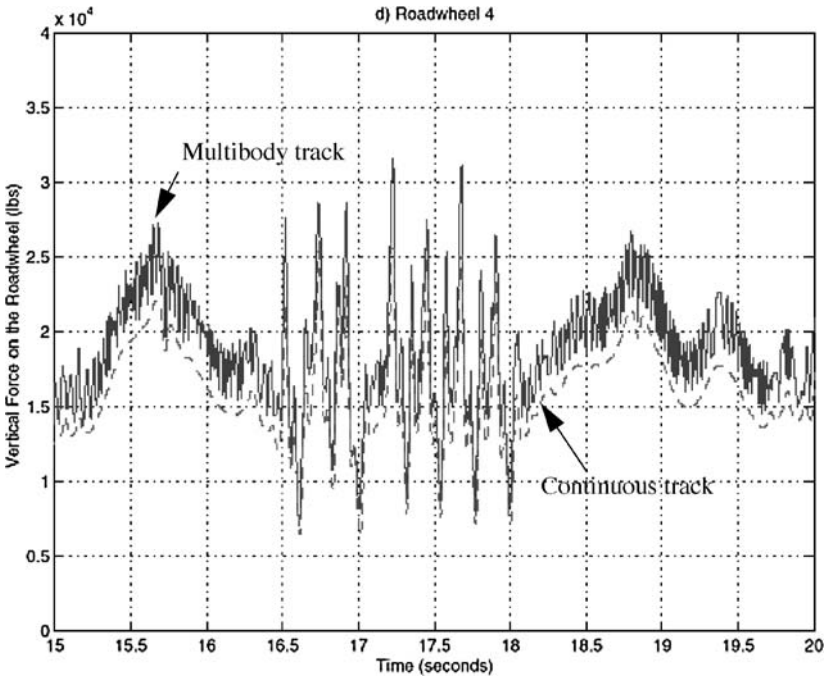

Figure 19. Comparison with the continuous track model.

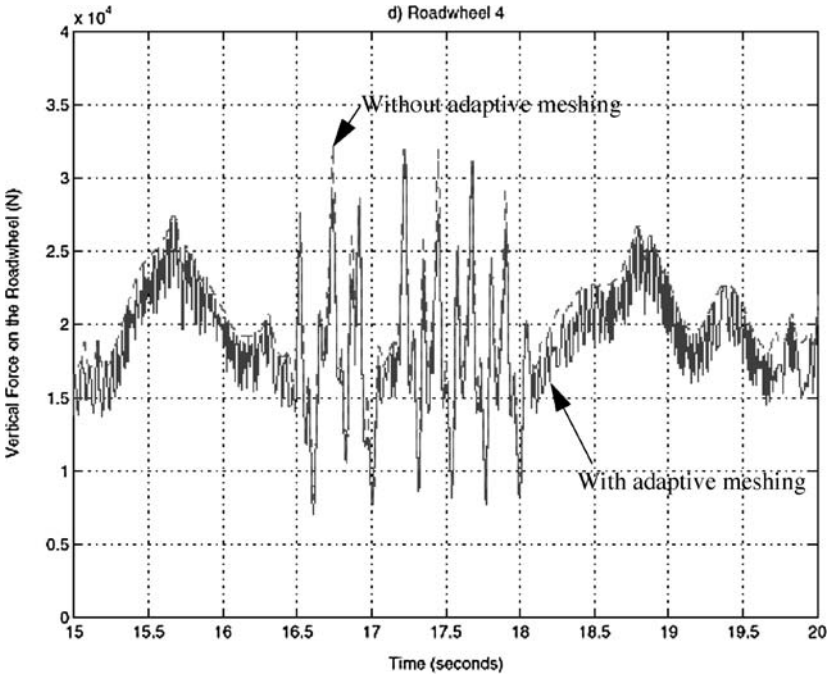

Figure 20. Comparison of results with and without adaptive meshing.

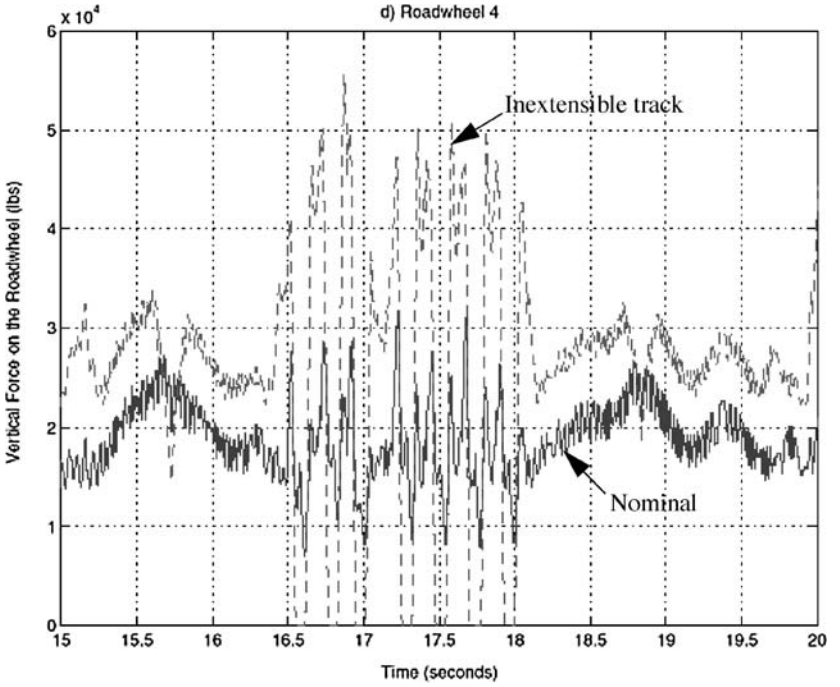

Figure 21. Comparison with the results of an (approximately) inextensible track.

track deflections. The resultant new track-wheel-terrain interaction model allows the computation of the track tension and the normal and shear forces at the track-terrain interface as the track negotiates terrain of arbitrary profile. The comparisons with the results obtained without using the current track-wheel-terrain interaction model have shown the great effectiveness of using the current model.

Acknowledgments

The authors acknowledge support provided by the U.S. Army Tank-Automotive Command (TACOM) through the University of Michigan Automotive Research Center, a U.S. Army Center of Excellence for Automotive Research, under contract number DAAE07-98-3-0022.

References

1. Ma, Z.-D. and Perkins, N.C., 'A track-wheel-terrain interaction model for dynamic simulation of tracked vehicles,' *Vehicle System Dynamics* **37**(6), 2002, 401–421.
2. Bekker, M.G., *Theory of Land Locomotion*. University of Michigan Press, Ann Arbor, MI, 1956.
3. Bekker, M.G., *Introduction to Terrain-Vehicle Systems*. University of Michigan Press, Ann Arbor, MI, 1969.
4. Wheeler, P., 'Tracked vehicle ride dynamics computer program,' SAE Paper 770048, 1977.
5. Doyle, G.R., Jr. and Workman, G.H. 'Prediction of track tension when traversing an obstacle,' SAE Paper 790416, 1979.
6. Garnich, M.R. and Grimm, T.R.,'Modeling and simulation of a tracked vehicle,' *ASME Proceedings of the International Computers in Engineering Conference and Exhibit on Advanced Automation* **2**, 1984, 591–600.
7. Dhir, A. and Sankar, S., 'Ride dynamics of high-speed tracked vehicles: simulation with field validation,' *Vehicle System Dynamics* **23**, 1994, 379–409.
8. Galaitsis, A.G., 'TRAXION: A model for predicting dynamic track loads in military vehicles,' *Transaction of ASME, Journal of Vibration, Acoustics, Stress, and Reliability in Design* **106**, 1984, 286–291.
9. Choi, J.H., Lee, H.C. and Shabana, A.A., 'Spatial dynamics of multibody tracked vehicles, part 1: spatial equations of motion,' *Vehicle System Dynamics* **29**, 1998, 27–49.
10. Choi, J.H., Lee, H.C. and Shabana, A.A., 'Spatial dynamics of multibody tracked vehicles, part 2: contact forces and simulation results,' *Vehicle System Dynamics* **29**, 1998, 113–137.
11. Wong, J.Y., Garber, M. and Preston-Thomas, J., 'Theoretical prediction and experimental substantiation of the ground pressure distribution and tractive performance of tracked vehicles,' *Proc. Instn Mech. Engrs* **198**(D15), 1984, 265–285.
12. Wong, J.Y., *Terramechanics and Off-Road Vehicles*. Amsterdam, The Netherlands, Elsevier Science Publishers B.V, 1989.
13. Wyk, D.J. van, Spoelstra, J. and Klerk, J.H. de, 'Mathematical modeling of the interaction between a tracked vehicle and the terrain,' *Appl. Math. Modeling* **20**, 1996, 838–846.
14. Gao, Y. and Wong, J.Y., 'The development and validation of a computer aided method for design evaluation of tracked vehicles with rigid links,' *Journal of Automobile Engineering* **208**, 1994, 207–215.

15. McCullough, M.K. and Haug, E.J., 'Dynamics of high mobility track vehicles,' *Journal of Mechanisms, Transmissions, and Automation in Design* **108**, 1986, 189–196.
16. Scholar, C. and Perkins, N.C., 'Longitudinal vibration of elastic vehicle track systems,' SAE Paper No.971090, 1997.
17. Scholar, C., Ma, Z.D. and Perkins, N.C., 'Modeling of tracked vehicles using a modal track representation: development and implementation,' Proceedings of SAE Noise and Vibration Conference, Traverse City, Michigan, 1999, SAE P-342, pp. 1061–1068.
18. Assanis, D.N., Bryzik, W., Castanier, M.P., Darnell, I.M., Filipi, Z.S., Hulbert, G.M., Jung, D., Ma, Z.-D., Perkins, N.C., Pierre, C., Scholar, C.M., Wang, W. and Zhang, G., 'Modeling and Simulation of an M1 Abrams Tank with advanced track dynamics and integrated virtual diesel engine,' *Mechanics of Structures and Machines* **27**(4), 1999, 453–505.
19. Janosi, Z. and Hanamoto, B., 'The analytical determination of drawbar pull as a function of slip for tracked vehicles in deformable soils,' *Proceedings of the First International Conference on Terrain-Vehicle Systems*, Torino, Italy, 1961.